

# “Superfast” Reaction in Turbulent Flow with Potential Disorder

Nga le Tran, Jeong-Man Park<sup>‡</sup>, and Michael W. Deem

Chemical Engineering Department, University of California, Los Angeles, CA  
90095-1592 USA

**Abstract.** We explore the regime of “superfast” reactivity that has been predicted to occur in turbulent flow in the presence of potential disorder. Computer simulation studies confirm qualitative features of the previous renormalization group predictions, which were based on a static model of turbulence. New renormalization group calculations for a more realistic, dynamic model of turbulence show that the superfast regime persists. This regime, with concentration decay exponents greater than that for a well-mixed reaction, appears to be a general result of the interplay among non-linear reaction kinetics, turbulent transport, and local trapping by potential disorder.

PACS numbers: 47.70.Fw, 82.20.Mj, 05.40.+j

Submitted to: *J. Phys. A: Math. Gen.*

<sup>‡</sup> Permanent address: Department of Physics, The Catholic University, Seoul, Korea

## 1. Introduction

Reactive turbulent flow is important in a variety of natural processes, ranging from the production of smog in the atmosphere[1] to the feeding habits of certain oceanic creatures[2]. The mixing effects of turbulence are put to use in a variety of engineering applications, including combustion reactors, fluid catalytic cracking units, and polymerization reactors. The behavior of reactive turbulent flow is usually analyzed, numerically or analytically, with the continuum reaction/transport equations [1, 3]. These mean-field equations fail, however, in two dimensions at low densities of reactants. This is understood in a general way, since the upper critical dimension for bimolecular reactions, even in the absence of turbulence, is two [4, 5, 6, 7].

A renormalization group treatment of a model of reactive turbulent flow has recently predicted a regime of “superfast” reactivity for the  $A+A \rightarrow \emptyset$  reaction in two dimensions [8]. The superfast reactivity occurs when a certain degree of quenched potential disorder is added to the turbulent system. In the superfast regime, the reactant concentration is predicted to decay more quickly than in a well-mixed reaction: *i.e.*  $c(t) \sim a/t^{1+x}$  at long times, with  $x > 0$ . This rapid decay occurs due to a subtle combination of the effects of turbulent transport, trapping by disorder, and reaction. It shows up in the analytical calculations as a renormalization of the effective reaction rate. It was anticipated that this result may have technological implications for certain thin-film reactors or fluidized MEMS devices.

The renormalization group calculations were carried out with a statistical model of turbulence, in the same spirit as in treatments of the turbulent transport of passive scalars [9, 10, 11]. A review of this approach to the dynamics of a passive scalar can be found in [12]. The statistics of the turbulent velocity field in the model were chosen to reproduce the correct transport properties at long times. There was freedom to choose either a time-dependent or time-independent velocity field, and the time-independent choice was made. This choice corresponds to G. I. Taylor’s hypothesis of frozen turbulence.

In this paper, we perform further studies to confirm the existence of the superfast reaction regime. In Section 2, we describe a method for simulating reactive turbulent flow with random, time-independent velocity fields. In Section 3, we present and discuss our computational results. The existence of the superfast regime is verified, and additional features arising from higher-loop contributions in the renormalization group are found. In Section 4, we present a renormalization group treatment of reactive turbulent flow with a more realistic, time-dependent model of the velocity field. When the appropriate type of potential disorder is included, the superfast regime is found to persist. We conclude in Section 5.

## 2. Simulation Methodology

We consider the reaction



occurring in a model of a two-dimensional, turbulent fluid. In the absence of reaction, the  $A$  particles are advected by the fluid streamlines. This chaotic motion is superimposed upon the natural Brownian motion of the particles. In addition, the particles experience a force due to the spatially-varying, random potential. In the presence of reaction, two  $A$  particles react with the conventional reaction rate constant  $\lambda$  when in contact.

We consider this reaction to proceed on a square  $N \times N$  lattice, both for computational convenience and to allow a direct comparison with the field-theoretic results. How the configuration of reactants on the lattice changes with time is specified by a master equation. The master equation defines transition rates for all of the possible changes to a given configuration of reactants on the lattice:

$$\begin{aligned} \frac{\partial P(\{n_i\}, t)}{\partial t} = & \sum_{ij} [\tau_{ji}^{-1}(n_j + 1)P(\dots, n_i - 1, n_j + 1, \dots, t) - \tau_{ij}^{-1}n_i P] \\ & + \frac{\lambda}{2h^2} \sum_i [(n_i + 2)(n_i + 1)P(\dots, n_i + 2, \dots, t) - n_i(n_i - 1)P] , \end{aligned} \quad (2)$$

where  $n_i$  is the number of  $A$  particles on lattice site  $i$ , and  $h$  is the lattice spacing. The rate of hopping from lattice site  $i$  to lattice site  $j$  is given by  $\tau_{ij}^{-1}$ , which will be defined below. The summation over  $i$  is over all sites on the lattice, and the summation over  $j$  is over all nearest neighbors of site  $i$ . The particles are initially placed at random on the lattice, with average density  $n_0$ . The initial concentration at any given site is, therefore, a Poisson random number:

$$\begin{aligned} P(n_i) &= \frac{[n_0 h^2]^{n_i}}{n_i!} e^{-n_0 h^2} \\ \langle n_i / h^2 \rangle &= n_0 . \end{aligned} \quad (3)$$

The turbulence and potential disorder enter this master equation through the hopping rates  $\tau_{ij}^{-1}$ . These rates are chosen so that the master equation reduces to the conventional transport equation when there is no reaction:

$$\frac{\partial c}{\partial t} = D \nabla^2 c + \beta D \nabla \cdot [c \nabla u - c \nabla \times \phi] , \quad (4)$$

where  $c(\mathbf{r}, t)$  is the concentration of the  $A$  particles,  $D$  is the diffusion constant,  $\beta = 1/(k_B T)$  is the inverse temperature,  $u(\mathbf{r})$  is the random potential, and  $\phi(\mathbf{r})$  is proportional to the random stream function. A particularly simple form for the transfer rate from position  $i = \mathbf{r}$  to the position  $j = \mathbf{r} + \Delta \mathbf{r}$  is

$$\tau_{ij}^{-1} = \frac{D}{h^2} [1 - \beta \Delta \mathbf{r} \cdot (\nabla u - \nabla \times \phi) / 2] . \quad (5)$$

When equation (5) is used in equation (2), one finds via a Taylor series expansion in  $h$  that the conventional transport equation (4) is reproduced. This form of the transfer

rates (5) is the one conventionally used in theoretical calculations [6]. In our simulations we choose, instead, to use the form

$$\tau_{ij}^{-1} = \frac{D}{h^2} \exp\{\beta(u_i - u_j)/2\} \exp\{\beta(\phi_{j'} - \phi_i)/2\} . \quad (6)$$

Here  $j$  and  $j'$  are nearest neighbors of site  $i$ . The identity of site  $j'$  is derived from site  $j$  by a counter-clockwise rotation of  $\pi/2$  about site  $i$ . This form leads to a transition rate in the simulation that is bounded and non-negative, in contrast to the simpler form of equation (5). A Taylor series expansion of equation (6) leads directly to the simpler equation (5). Since both of these forms are equivalent in the limit of a small lattice spacing, they are expected to lead to identical scaling in the long-time regime.

Following the usual statistical approach to turbulence, we take the stream function and potential to be Gaussian random variables with correlation functions given by

$$\begin{aligned} \hat{\chi}_{\phi\phi}(\mathbf{k}) &= \frac{\sigma}{k^{2+y}} \\ \hat{\chi}_{uu}(\mathbf{k}) &= \frac{\gamma}{k^{2+y}} , \end{aligned} \quad (7)$$

where the Fourier transform of a function in two dimensions is given by  $\hat{f}(\mathbf{k}) = \int d^2\mathbf{r} f(\mathbf{r}) \exp(i\mathbf{k} \cdot \mathbf{r})$ . The random stream function and potential are generated first in Fourier space, where the values at different wave vectors are independent Gaussian random variables, and then converted to real space with a fast Fourier transform [13]. Periodic boundary conditions are used on the lattice. The quality of the random number generator is of importance when simulating systems with long-ranged correlations [13]. We use a sum of three linear congruential generators method [14].

Isotropic, fully-developed turbulence is modeled by  $y = 8/3$  and  $\gamma = 0$ . Developing turbulence is modeled by smaller, positive values of  $y$ . Potential disorder of the form we consider here could arise in a reaction between ionic species confined to a thin film of fluid between spatially-addressable electrodes or media with quenched, charged disorder. The ionic species would move in the random potential generated by the electrodes or quenched disorder. The electrodes or quenched disorder could be devised so as to reproduce the correlation function  $\chi_{uu}(r)$ .

The master equation (2) can be exactly solved by a Markov Poisson process [15]. In such a process, we consider the motion of discrete  $A$  particles on the lattice. For any given configuration of reactants at time  $t$ , there are  $4 \sum_i n_i$  possible hopping events. Each occurs with a rate given by equation (6). In addition, there are  $\sum_i n_i(n_i - 1)/2$  possible reaction events on the lattice. Each of these occurs with the rate  $\tau_{\text{rxn}}^{-1} = \lambda/h^2$ .

The Markov process is started by initially placing the reactants on the lattice at random with average density  $n_0$ . Each step of the Markov process consists of randomly picking one of the possible reaction or diffusion events and incrementing time appropriately. The probability of event  $\alpha$  occurring, out of all the possible diffusion and reaction moves, is

$$P(\text{event } \alpha) = \frac{\tau_{\alpha}^{-1}}{\sum_{\gamma} \tau_{\gamma}^{-1}} . \quad (8)$$

After performing the chosen event, time is incremented by

$$\Delta t = \frac{-\log \zeta}{\sum_{\gamma} \tau_{\gamma}^{-1}}, \quad (9)$$

where  $\zeta$  is a random number uniformly distributed between 0 and 1. The Markov chain is continued until zero or one reactants remain on the lattice, at which point no more reaction events will occur.

This Markov process, when averaged over initial conditions and trials, exactly reproduces the predictions of the master equation. Averages over the statistics of the turbulence and potential disorder are taken by directly averaging over sufficiently many instances of the random fields. Since the asymptotic scaling regime is reached only for long times, we make two approximations to facilitate the computations. First, we set the reaction rate to infinity. That is, when a particle moves to a site with another particle already present, the reaction occurs immediately. Physically, we do not expect this to modify the long-time decay law, since at long times the reaction will be in a transport-limited regime. Indeed, the renormalization group prediction for the decay exponent is independent of the reaction rate [8]. The predicted prefactor also has a well-defined value in the infinite reaction rate limit. Second, we assume that each particle on the lattice is equally likely to undergo a hopping event:

$$P(\text{moving particle } \alpha) = \frac{1}{n}, \quad (10)$$

where  $n = \sum_i n_i$  is the total number of particles on the lattice. After the particle to move is chosen, the probabilities of each of the four possible hopping events are derived from equation (6). In particular, another uniform random number is generated for comparison against the four different hop probabilities:

$$P(\text{hop } i) = \frac{\tau_i^{-1}}{\sum_j \tau_j^{-1}}. \quad (11)$$

After the chosen hop is performed, time is incremented by  $\Delta t = N^2 / (n \sum_{ij} \tau_{ij}^{-1})$ . The uniform choice of particles to move and the approximate time incrementation are not expected to influence the long-time exponents. In particular, these approximations are exact in the long-time limit if the hopping rates of equation (5) are used.

### 3. Simulation Results and Discussion

The renormalization group calculations make a prediction for the concentration decay exponent, the  $\alpha$  in  $c(t) \sim at^{-\alpha}$  [8]. The predictions depend on the properties of the turbulence and potential disorder through the parameters  $y$ ,  $\sigma$ , and  $\gamma$ . The predictions for several values of  $y$  are shown in figure 1. The decay exponent initially rises with increasing potential disorder and eventually decreases. The maximum reaction rate of  $\alpha = 1 + y/(6 - y)$  occurs for  $\sigma = 3\gamma$ . The decay rate depends on  $\sigma$  and  $\gamma$  only through the combination  $\gamma/\sigma$ . These predictions come from a one-loop renormalization group calculation, and they are strictly valid only for small  $y$ . In addition, the predictions

should be more accurate for small  $\gamma$ , because it is known that higher-loop corrections lead to a modification of the flow diagram for large  $\gamma$ .

We find that our Poisson process efficiently solves the master equation for values of  $y$  near unity. For smaller values of  $y$ , the renormalization of the effective reaction rate occurs slowly. This means that the predicted asymptotic scaling occurs only at long times, times longer than we can reach in our simulation. For larger values of  $y$ , significant lattice effects occur, due to our choice of transition rates, equation (6), and correlation functions, equation (7).

Shown in figure 2 are the decay exponents observed in our simulation for  $y = 3/4$ . The decay exponents observed for  $y = 1$  and  $y = 5/4$  are shown in figures 3 and 4, respectively. Each of the data points in the figure is an average over three different runs on three different instances of the turbulence and potential disorder. The standard deviations estimated from these three runs are shown as the error bars.

We made a few canonical choices for constants in our simulation. So as to reach the asymptotic scaling regime, we used  $4096 \times 4096$  square lattices. Simulations on  $2048 \times 2048$  lattices gave similar results. Finite size effects should be most noticeable for small values of  $y$ ,  $\sigma$ , or  $\gamma$ , since in that regime the renormalization of the effective reaction rate is most slow. Indeed, finite size effects only appear to be present in figure 2 for small  $\gamma/\sigma$ , where the slow renormalization of  $\lambda(l)$  leads to an observed decay exponent that is below the correct asymptotic value of unity. While additional finite size effects could be present, the agreement at small  $\gamma/\sigma$  among curves for different  $\sigma$  but same  $\gamma/\sigma$  and  $y$ , and the agreement between the results for  $2048 \times 2048$  and  $4096 \times 4096$  lattices, argues against this. We used a lattice spacing of  $h = 1$ , which we can enforce by a spatial rescaling, and a diffusion constant of  $D = 1$ , which we can enforce by a temporal rescaling. The long-time decay exponent is not affected by these rescalings. We collected the time-dependent concentration data on the lattice by binning the results into a histogram with a temporal bin width of  $\delta t = 1$ . We continued each simulation until the concentration was so low,  $c \approx (\text{const})/N^2$ , that lattice effects were obvious. We show in figure 5 the simulation results for a typical run. The average of the slopes determined in three such runs gives one of the data points in figures 2-4.

Since the renormalization group predictions depend only on  $\gamma/\sigma$ , we fixed  $\sigma$  and varied  $\gamma$  for each simulation at a fixed value of  $y$ . Under these conditions, the effective strength of turbulence is expected to flow to its fixed point value,  $\sigma \rightarrow \sigma^* \approx 2\pi y(2\pi/h)^y$  [8]. In each of the figures 2-4 we show results for three different “bare” values of  $\sigma$ :  $\sigma = \sigma^*$ ,  $\sigma = \sigma^*/2$ , and  $\sigma = 3\sigma^*/2$ .

We use a  $\ln c(t)$  versus  $\ln t$  plot to obtain the decay exponent. This plot has many more data at large  $\ln t$ , which leads to an over-weighting of the long-time regime. To counteract this effect, we use data exponentially spaced in time. We exclude both short-time data, which are not in the asymptotic regime, and long-time data, which show finite-size effects. Use of exponentially spaced data allows one to obtain a reliable estimate of the error in the exponent determined for a given realization of the disorder. We find that this statistical error is smaller than the systematic deviation that occurs

for each different realization of the disordered streamlines and potential. The error bars shown in the figures encompass both the statistical and the systematic errors.

We see that there is a general agreement between the simulation results and the renormalization group predictions. In particular, the superfast reaction regime,  $\alpha > 1$ , is observed. This was a dramatic analytical prediction, and confirmation of this regime is significant. The exponent is observed to reach roughly the maximum value of  $1+y/(6-y)$  predicted by theory.

The agreement between the simulation results and the one-loop renormalization group predictions is better for smaller  $y$ . For small  $y$ , the location of the peak in reactivity is trending towards the predicted value of  $\gamma/\sigma = 1/3$ . For finite values of  $y$ , the location of the peak is shifted to the left. Indeed, the whole curve is shifted to the left for finite  $y$ . One consequence of this is that the observed decay exponent decreases below unity for  $\gamma/\sigma$  close to, but less, than one, in contrast to the one-loop predictions.

The agreement between the simulation results and the one-loop predictions is also better for small  $\gamma$ . For small  $\gamma/\sigma$ , the simulation results for different values of  $\sigma$  fall on the same curve. This is the universal curve predicted at one-loop, albeit compressed to the left. For large  $\gamma$ , the simulation results depend on both  $\gamma$  and  $\sigma$ , not simply on the ratio  $\gamma/\sigma$ . This dependence is presumably due to corrections that would enter in a higher-loop calculation.

#### 4. Renormalization Group Treatment of Dynamic Turbulence

The simulations, and the previous renormalization group calculations, were performed for a model of turbulence with streamlines random in space, but constant in time. For this model, both the analytical and computational studies predict a regime of superfast reaction in the presence of potential disorder. This regime was understood to occur as a general consequence of the interplay among turbulent transport, trapping by the random potential, and a non-linear dependence of the reaction rate on local reactant concentration. This regime was not believed to occur, for example, due to some subtle, artificial interaction between the quenched potential and quenched streamlines.

Even so, it would be interesting to predict the existence of the superfast reaction regime for a dynamic model of turbulence. As we have seen, reliable simulations require large lattices and long times, even for quenched turbulence. Moreover, simulations were possible only for an intermediate range of  $y$ , due to the competing considerations of minimizing lattice effects and accessing the asymptotic regime. Renormalization group theory is, however, a viable approach to studying reactive turbulent flow in a dynamic model of turbulence.

We, again, use a statistical model of turbulence [11]. We now assume that the stream function is random in both space and time:

$$\hat{\chi}_{\phi\phi}(\mathbf{k}, t_1 - t_2) = \frac{\sigma}{k^{2+y\sigma}} |t_1 - t_2|^{-\rho} \Theta(t_1 - t_2) , \quad (12)$$

where  $\Theta(t)$  is the Heavyside step function. A family of models for turbulence is generated

by varying  $\rho$  and  $y_\sigma$ . Isotropic turbulence is modeled when  $3y_\sigma - 2\rho = 8$ , at least for small  $\rho$ . We include a random potential, as before:

$$\hat{\chi}_{uu}(\mathbf{k}) = \frac{\gamma}{k^{2+y_\gamma}} . \quad (13)$$

We will find that the most interesting regime occurs for  $y_\gamma < y_\sigma$ , due to the weakening of the random stream function through decorrelation over time.

As in previous studies [8], we map the master equation (2) onto a field theory using the coherent state representation [4, 16]. For this operation, we use the transition rates given by equation (5). The random and stream function are incorporated with the replica trick [10], using  $N$  replicas of the original problem. The concentration of reactants at time  $t$ , averaged over the initial conditions,  $c(\mathbf{r}, t)$ , is given by

$$c(\mathbf{r}, t) = \lim_{N \rightarrow 0} \langle a(\mathbf{r}, t) \rangle , \quad (14)$$

where the average is taken with respect to  $\exp(-S)$ , with

$$\begin{aligned} S = & \sum_{\alpha=1}^N \int d^2\mathbf{r} \int_0^{t_f} dt \bar{a}_\alpha(\mathbf{r}, t) [\partial_t - D\nabla^2 + \delta(t)] a_\alpha(\mathbf{r}, t) \\ & + \frac{\lambda}{2} \sum_{\alpha=1}^N \int d^2\mathbf{r} \int_0^{t_f} dt \left[ 2\bar{a}_\alpha(\mathbf{r}, t) a_\alpha^2(\mathbf{r}, t) + \bar{a}_\alpha^2(\mathbf{r}, t) a_\alpha^2(\mathbf{r}, t) \right] \\ & - n_0 \sum_{\alpha=1}^N \int d^2\mathbf{r} \bar{a}_\alpha(\mathbf{r}, 0) \\ & - \frac{\beta^2 D^2}{2} \sum_{\alpha_1, \alpha_2=1}^N \int dt_1 dt_2 \int_{\mathbf{k}_1 \mathbf{k}_2 \mathbf{k}_3 \mathbf{k}_4} (2\pi)^2 \delta(\mathbf{k}_1 + \mathbf{k}_2 + \mathbf{k}_3 + \mathbf{k}_4) \\ & \times \hat{a}_{\alpha_1}(\mathbf{k}_1, t_1) \hat{a}_{\alpha_1}(\mathbf{k}_2, t_1) \hat{a}_{\alpha_2}(\mathbf{k}_3, t_2) \hat{a}_{\alpha_2}(\mathbf{k}_4, t_2) \\ & \times \left[ \mathbf{k}_1 \cdot (\mathbf{k}_1 + \mathbf{k}_2) \mathbf{k}_3 \cdot (\mathbf{k}_3 + \mathbf{k}_4) \hat{\chi}_{uu}(|\mathbf{k}_1 + \mathbf{k}_2|) \right. \\ & \left. + \mathbf{k}_1 \times \mathbf{k}_2 \mathbf{k}_3 \times \mathbf{k}_4 \hat{\chi}_{\phi\phi}(|\mathbf{k}_1 + \mathbf{k}_2|, t_2 - t_1) \right] . \quad (15) \end{aligned}$$

The notation  $\int_{\mathbf{k}}$  stands for  $\int d^2\mathbf{k}/(2\pi)^2$ . The upper time limit in the action is required only to satisfy  $t_f \geq t$ .

Using renormalization group theory, we can derive the flow equations for this model. We find that the turbulence contributes directly to the dynamical exponent, and therefore to the transport properties, but not directly to the effective reaction rate. The potential disorder contributes directly to both the dynamical exponent and the effective reaction rate. Finally, the dynamical exponent contributes indirectly to the effective reaction rate as well. We define  $g_\sigma = \beta^2 \sigma \Lambda^{2\rho - y_\sigma} D^\rho \Gamma(1 - \rho)/(4\pi)$  and  $g_\gamma = \beta^2 \gamma \Lambda^{-y_\gamma}/(4\pi)$ , where  $\Lambda = 2\pi/h$  is the cutoff in Fourier space, and  $\Gamma(x)$  is the standard Gamma function. The precise definition of  $g_\sigma$  depends on the regularization of  $\chi_{\phi\phi}$  at  $t = 0$ . At one loop, we find the flow equations to be

$$\frac{d \ln n_0}{dl} = 2$$



$$\begin{aligned}
 \frac{d \ln \lambda}{dl} &= -\frac{\lambda}{4\pi D} + 3g_\gamma - g_\sigma \\
 \frac{d \ln g_\gamma}{dl} &= y_\gamma - 2g_\sigma \\
 \frac{d \ln g_\sigma}{dl} &= y_\sigma - \rho z - 2g_\sigma .
 \end{aligned}
 \tag{16}$$

The dynamical exponent is given by

$$z = 2 + g_\gamma - g_\sigma . \tag{17}$$

To achieve the superfast regime, we must set  $y_\gamma = y_\sigma - \rho z$ . Without this choice, the potential disorder will either dominate or be irrelevant. It is natural that the appropriate  $y_\gamma$  should be weaker than  $y_\sigma$ , since the effective turbulence strength is weakened by decorrelation effects over time. With this choice, we find that the ratio  $g_\gamma(l)/g_\sigma(l)$  remains constant under the renormalization group flows. The parameter  $g_\sigma(l)$ , however, flows to the fixed point  $g_\sigma^* = y_\gamma/2$ . Moreover, we find that when  $g_\gamma/g_\sigma > 1/3$ , the effective reaction rate flows to a finite fixed point  $\lambda^* = 4\pi D(3g_\gamma^* - g_\sigma^*)$ . When  $g_\gamma/g_\sigma < 1/3$ , the effective reaction rate renormalizes to zero.

With the choice of  $y_\gamma = y_\sigma - \rho z$ , the flow equations are the same as for the static model of turbulence [8]. The matching is the same, as well. In terms of these new variables, therefore, the predicted concentration dependence is the same. *In particular, the superfast reaction regime is predicted to exist for this dynamic model of turbulence.* The explicit, long-time concentration dependence for weak disorder is

$$c(t) \sim \left[ \frac{1}{4\pi D(g_\sigma^* - 3g_\gamma^*)} + \frac{1}{\lambda_0} \right] \frac{1}{t} \left( \frac{t}{t_0} \right)^{-2g_\gamma^*/(2+g_\gamma^*-g_\sigma^*)}, \quad (3g_\gamma < g_\sigma), \tag{18}$$

where  $\lambda_0$  is the bare value of the reaction rate. The matching time,  $t_0$ , is given roughly by  $t_0 \approx h^2/(2D)$ . For strong disorder, the concentration decays as

$$c(t) \sim \frac{1}{4\pi D(3g_\gamma^* - g_\sigma^*)t} \left( \frac{t}{t_0} \right)^{(g_\gamma^*-g_\sigma^*)/(2+g_\gamma^*-g_\sigma^*)}, \quad (3g_\gamma > g_\sigma). \tag{19}$$

At the location of the maximum reaction rate, there is a logarithmic correction to power-law decay:

$$c(t) \sim \frac{\ln(t/t_0)}{8\pi(1 - y_\gamma/6)Dt} t^{-y_\gamma/(6-y_\gamma)}, \quad (3g_\gamma = g_\sigma). \tag{20}$$

## 5. Conclusion

A regime of reaction rates faster than that for a well-mixed reaction was observed in simulations of a static model of turbulence plus potential disorder. Qualitative predictions of previous renormalization group studies of this model were reproduced. Interesting departures from the one-loop predictions, such as a compression of the decay exponent curve to the left, were observed. These features are expected to be reproduced in higher-loop analytical calculations.

Renormalization group calculations for a more realistic, dynamic model of turbulence show that the superfast regime persists. Indeed, these calculations suggest that our general understanding of the phenomenon of superfast reactivity is correct. The random potential tends to attract reactants to localized regions in space, and by doing so increases the reaction rate in a non-linear manner in these regions. The reactants, therefore, annihilate at a faster than average rate in these regions. The turbulent velocity fields transport reactants to these regions rapidly, although the transport is slowed by the ruggedness of the random potential landscape. The net effect of the trapping and the turbulent transport is superfast reactivity whenever the mean-square displacement is super-linear.

The existence of a superfast reaction regime is of great interest from a practical point of view. Often, it is assumed in reactor design that the highest reaction rate is obtained for a well-mixed system [17]. Our results show that under certain conditions, the highest reaction rate is achieved, instead, for an inhomogeneous system. This behavior has been observed experimentally. Indeed, an enhancement due to inhomogeneous reactant concentrations of the effective reaction rate between ions in a chaotically-mixed, two-dimensional, fluid with attractors has recently been observed [18]. The superfast regime may be relevant to a variety of reactors, including thin-film reactors, certain combustion reactors, and certain types of micro-electro-mechanical (MEMS) devices.

## Acknowledgments

This research was supported by the National Science Foundation through grants CHE-9705165 and CTS-9702403.

- [1] R. W. Bilger, L. R. SaeTRAN, and L. V. Krishnamoorthy, *J. Fluid Mech.* **233**, 211 (1991).
- [2] T. Kjørboe and E. Saiz, *Mar. Ecol. Prog. Ser.* **122**, 135 (1995).
- [3] J. C. Hill, *Ann. Rev. Fluid Mech.* **8**, 135 (1976).
- [4] L. Peliti, *J. Phys. A: Math. Gen.* **19**, L365 (1986).
- [5] B. P. Lee and J. Cardy, *J. Stat. Phys.* **80**, 971 (1995); **87**, 951 (1997).
- [6] J.-M. Park and M. W. Deem, *Phys. Rev. E* **57**, 3618 (1998).
- [7] M. W. Deem and J.-M. Park, *Phys. Rev. E* **57**, 2681 (1998).
- [8] M. W. Deem and J.-M. Park, *Phys. Rev. E* **58**, 3223 (1998).
- [9] D. S. Fisher, M. P. A. Fisher, and D. A. Huse, *Phys. Rev. B* **43**, 130 (1991).
- [10] V. E. Kravtsov, I. V. Lerner, and V. I. Yudson, *J. Phys. A: Math. Gen.* **18**, L703 (1985).
- [11] M. Avellaneda and A. J. Majda, *Phys. Rev. Lett.* **68**, 3028 (1992).
- [12] J. P. Bouchaud and A. Georges, *Phys. Rep.* **195**, 127 (1990).
- [13] V. Pham and M. W. Deem, *J. Phys. A: Math. Gen.* **31**, 7235 (1998).
- [14] B. Wichmann and D. Hill, *Byte* **12**, 127 (1987).
- [15] T. Elston and C. Doering, *J. Stat. Phys.* **83**, 359 (1996).
- [16] B. P. Lee, *J. Phys. A: Math. Gen.* **27**, 2633 (1994).
- [17] K. Jensen, *Nature* **393**, 735 (1998).
- [18] O. Paireau and P. Tabeling, *Phys. Rev. E* **56**, 2287 (1997).

**Figure Captions**

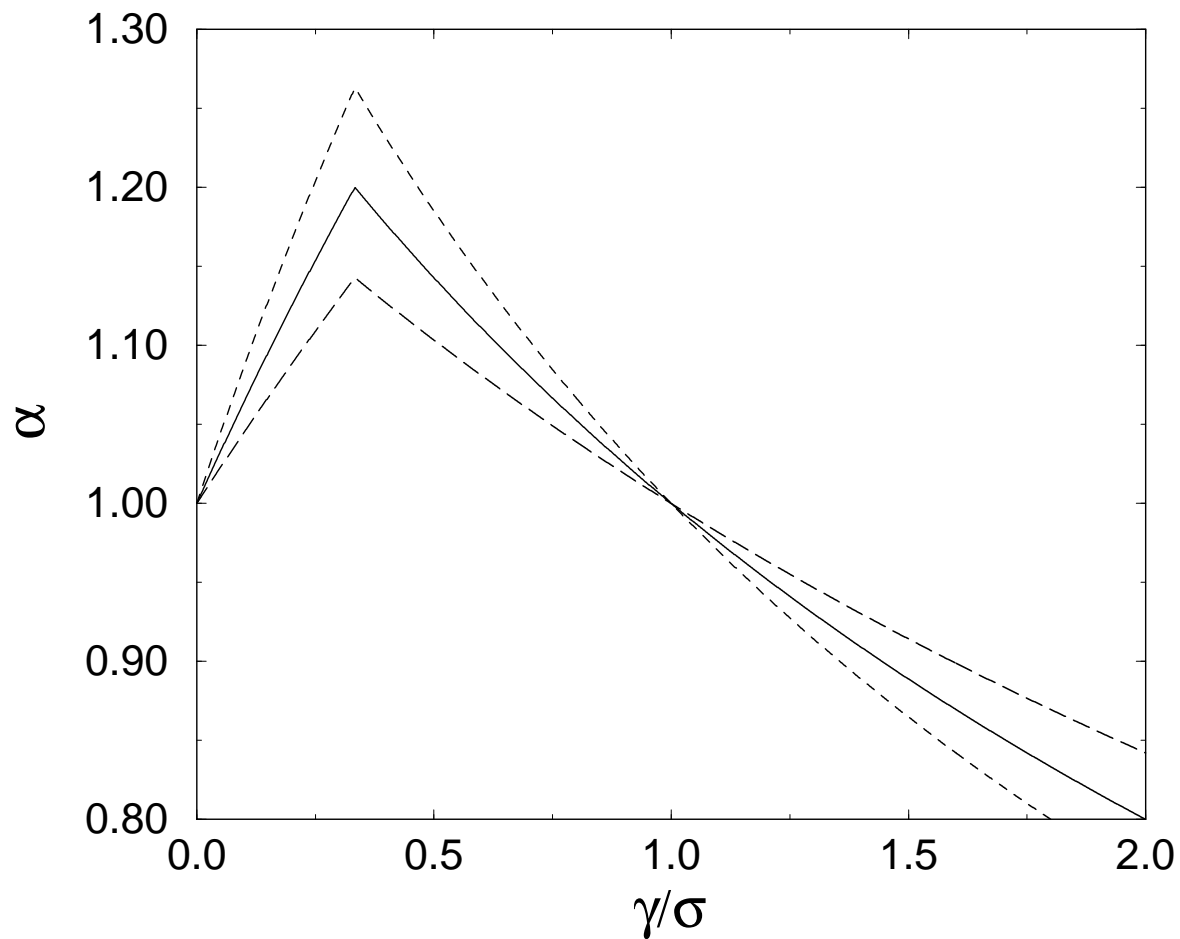


**Figure 1.** The decay exponent for the  $A + A \rightarrow \emptyset$  reaction:  $c(t) \sim (\text{const})t^{-\alpha}$ . The correspond to  $y = 1$  (solid),  $y = 5/4$  (short-dashed), and  $y = 3/4$  (long-dashed).

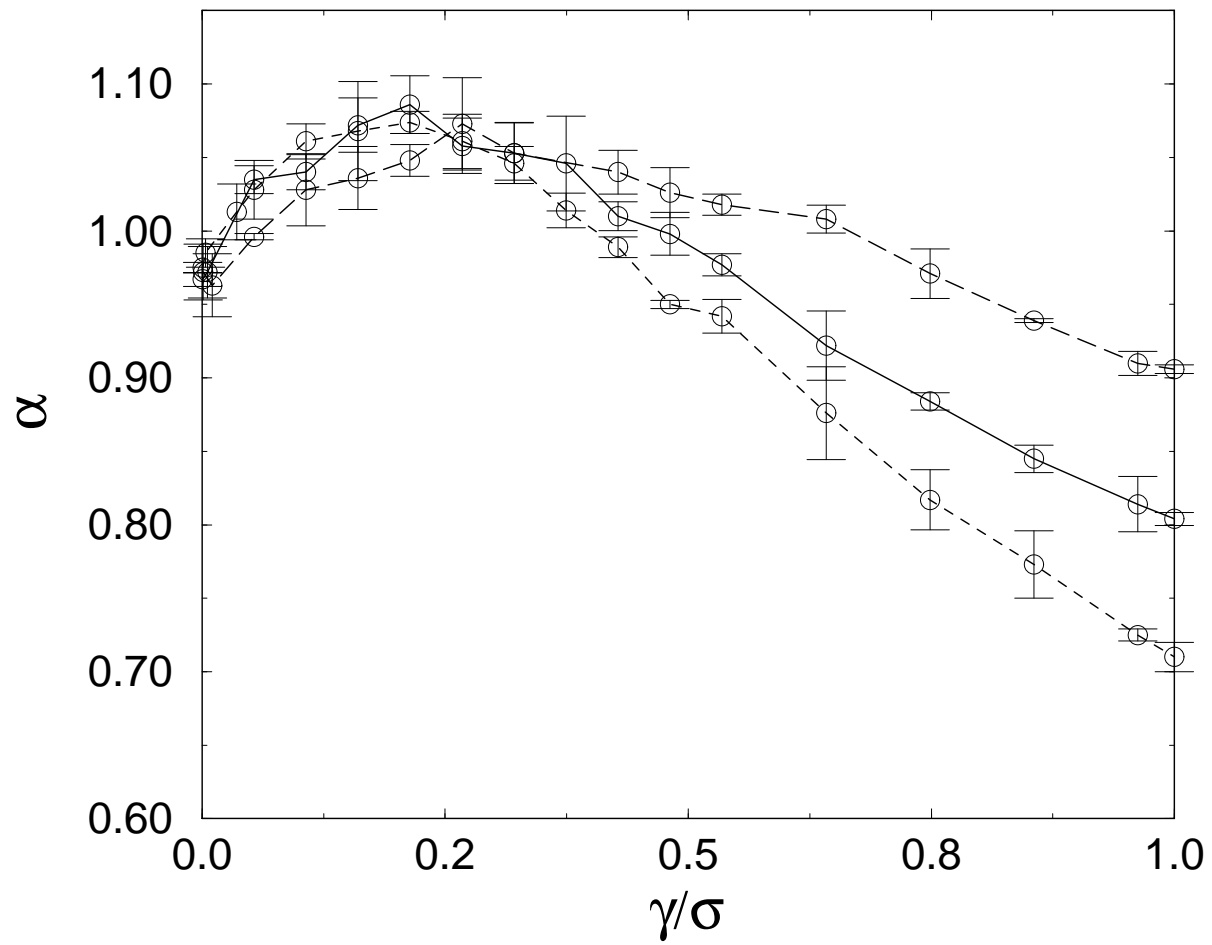


**Figure 2.** The decay exponent observed in the simulation for  $y = 3/4$ . The three curves correspond to  $\sigma = \sigma^*$  (solid),  $\sigma = 3\sigma^*/2$  (short-dashed), and  $\sigma = \sigma^*/2$  (long-dashed).

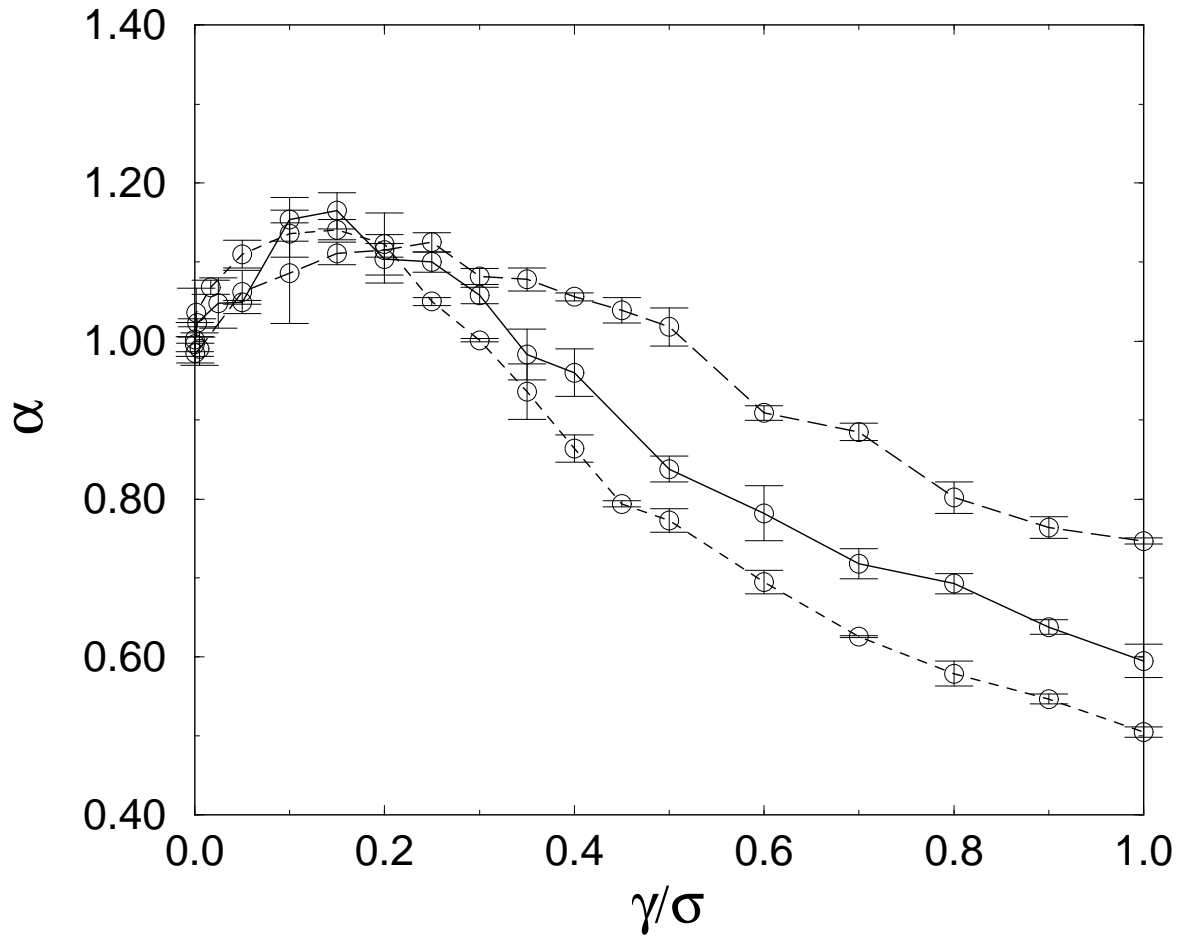


**Figure 3.** The decay exponent observed in the simulation for  $y = 1$ . The three curves correspond to  $\sigma = \sigma^*$  (solid),  $\sigma = 3\sigma^*/2$  (short-dashed), and  $\sigma = \sigma^*/2$  (long-dashed).

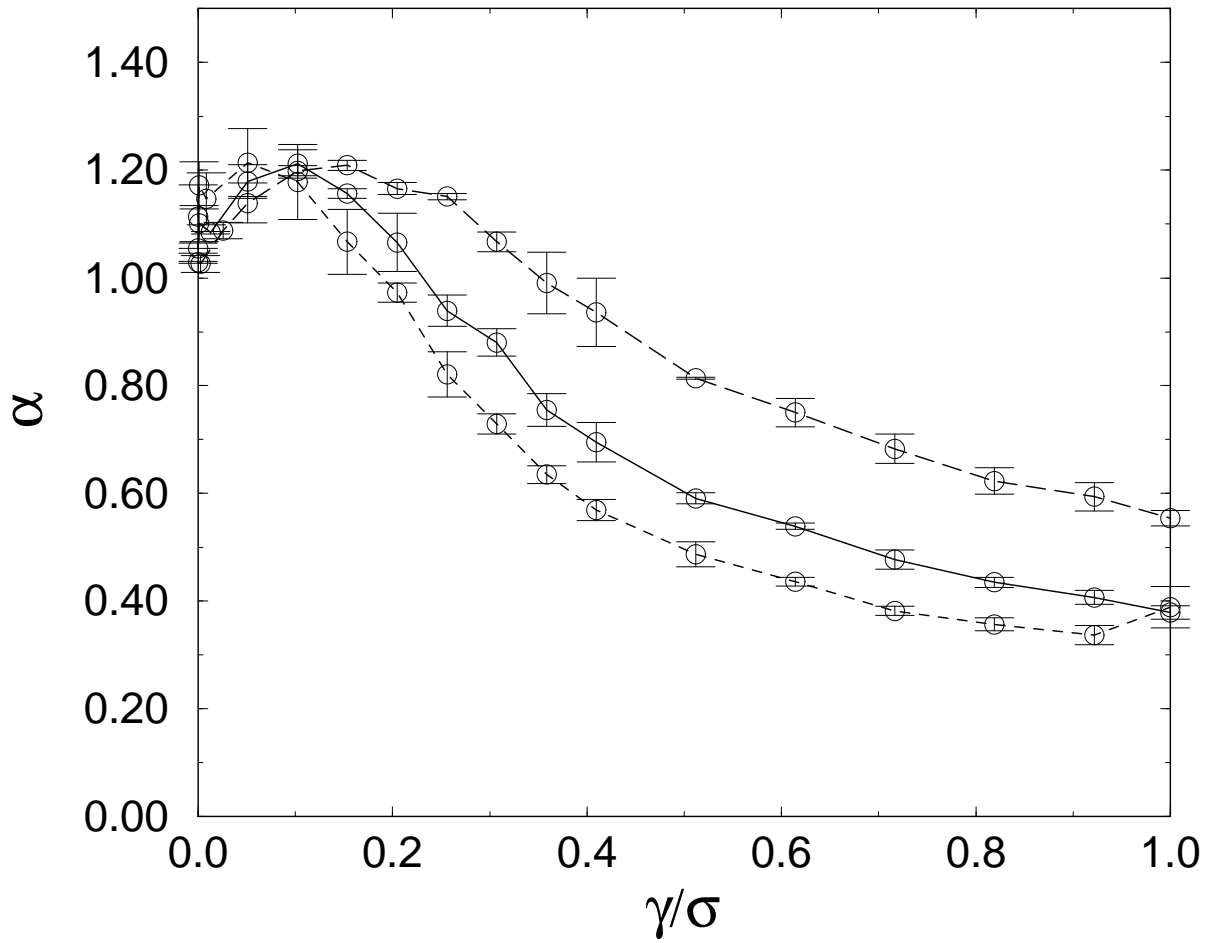


**Figure 4.** The decay exponent observed in the simulation for  $y = 5/4$ . The three curves correspond to  $\sigma = \sigma^*$  (solid),  $\sigma = 3\sigma^*/2$  (short-dashed), and  $\sigma = \sigma^*/2$  (long-dashed).

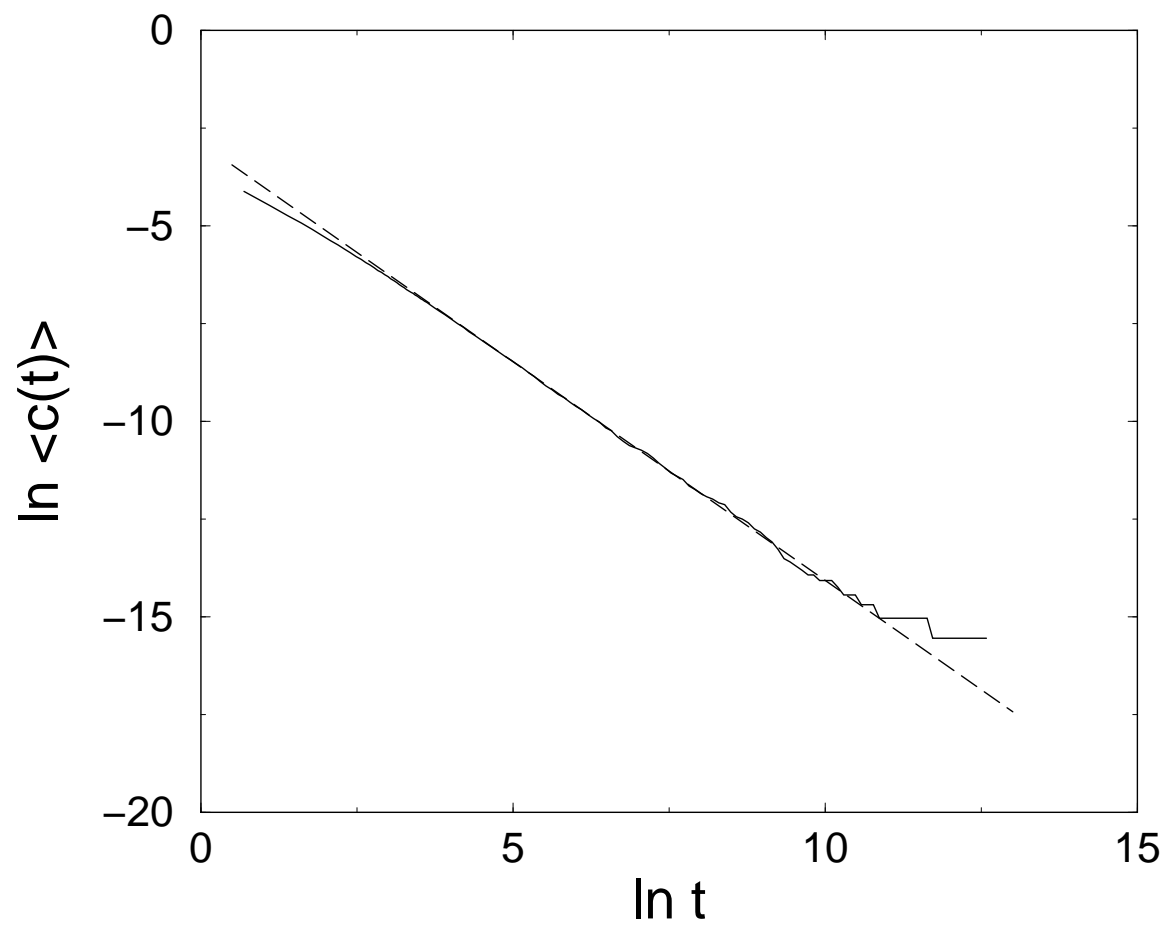


**Figure 5.** The concentration as a function of time (solid line) for the case  $y = 1$ ,  $\sigma = \sigma^*$ , and  $\gamma/\sigma = 0.2$ . Also shown is the fit to the data in the scaling regime (dashed line).